

Dynamical signatures of the one-dimensional deconfined quantum critical point

Ning Xi(西宁) and Rong Yu(俞榕)†

Citation: Chin. Phys. B, 2022, 31 (**5**): 057501. DOI: 10.1088/1674-1056/ac5987
Journal homepage: http://cpb.iphy.ac.cn; http://iopscience.iop.org/cpb

What follows is a list of articles you may be interested in

Structure and frustrated magnetism of the two-dimensional triangular lattice antiferromagnet $Na_2BaNi(PO_4)_2$

Fei Ding(丁飞), Yongxiang Ma(马雍翔), Xiangnan Gong(公祥南), Die Hu(胡蝶), Jun Zhao(赵俊), Lingli Li(李玲丽), Hui Zheng(郑慧), Yao Zhang(张耀), Yongjiang Yu(于永江), Lichun Zhang(张立春), Fengzhou Zhao(赵风周), and Bingying Pan(泮丙营)

Chin. Phys. B, 2021, 30 (**11**): 117505. DOI: 10.1088/1674-1056/abff1d

Spin correlations in the *S=1* armchair chain Ni_2NbBO_6 as seen from NMR

Kai-Yue Zeng(曾凯悦), Long Ma(马龙), Long-Meng Xu(徐龙猛), Zhao-Ming Tian(田召明), Lang-Sheng Ling(凌浪生), and Li Pi(皮雳)

Chin. Phys. B, 2021, 30 (**4**): 047503. DOI: 10.1088/1674-1056/abc2b5

Interplay between spin frustration and magnetism in the exactly solved two-leg mixed spin ladder

Yan Qi(齐岩), Song-Wei Lv(吕松玮), An Du(杜安), Nai-sen Yu(于乃森)

Chin. Phys. B, 2016, 25 (**11**): 117501. DOI: 10.1088/1674-1056/25/11/117501

Spin frustration and magnetic ordering in triangular lattice antiferromagnet $Ca_3CoNb_2O_9$

Dai Jia, Zhou Ping, Wang Peng-Shuai, Pang Fei, Tim J. Munsie, Graeme M. Luke, Zhang Jin-Shan, Yu Wei-Qiang

Chin. Phys. B, 2015, 24 (**12**): 127508. DOI: 10.1088/1674-1056/24/12/127508

Exchange coupling and helical spin order in the triangular lattice antiferromagnet $CuCrO_2$ using first principles

Jiang Xue-Fan, Liu Xian-Feng, Wu Yin-Zhong, Han Jiu-Rong

Chin. Phys. B, 2012, 21 (**7**): 077502. DOI: 10.1088/1674-1056/21/7/077502

RAPID COMMUNICATION

Dynamical signatures of the one-dimensional deconfined quantum critical point

Ning Xi(西宁) and Rong Yu(俞榕)†

Department of Physics and Beijing Key Laboratory of Opto-electronic Functional Materials and Micro-nano Devices, Renmin University of China, Beijing 100872, *China*

(Received 29 December 2021; revised manuscript received 26 February 2022; accepted manuscript online 2 March 2022)

We study the critical scaling and dynamical signatures of fractionalized excitations at two different deconfined quantum critical points (DQCPs) in an $S = 1/2$ spin chain using the time evolution of infinite matrix product states. The scaling of the correlation functions and the dispersion of the conserved current correlations explicitly show the emergence of enhanced continuous symmetries at these DQCPs. The dynamical structure factors in several different channels reveal the development of deconfined fractionalized excitations at the DQCPs. Furthermore, we find an effective spin–charge separation at the DQCP between the ferromagnetic (FM) and valence bond solid (VBS) phases, and identify two continua associated with different types of fractionalized excitations at the DQCP between the X-direction and Z-direction FM phases. Our findings not only provide direct evidence for the DQCP in one dimension but also shed light on exploring the DQCP in higher dimensions.

Keywords: one-dimensional antiferromagnetism, spin frustration, deconfined quantum critical point, spin dynamics, infinite time-evolving block decimation

PACS: 75.10.Kt, 75.40.Gb **DOI:** 10.1088/1674-1056/ac5987

1. Introduction

Significant quantum fluctuations in low-dimensional spin frustrated systems can give rise to novel quantum phases and exotic quantum phase transitions.[1–5] One substantial difference from the classical systems is that in these quantum spin systems, some phases can not be characterized by conventional order parameters with broken symmetry. Correspondingly, quantum phase transitions may be beyond the standard Landau–Ginzburg–Wilson (LGW) paradigm. Surprisingly, even when the ordered phases can be described by conventional order parameters with spontaneous symmetry breaking (SSB), the quantum phase transition between them may still be exotic and beyond the LGW paradigm. One of the most attractive examples is the DQCP between the Néel antiferromagnetic (AFM) and VBS states in two dimensions, proposed by Senthil *et al.*[6,7] Landau theory dictates a first-order VBS–AFM transition because the order parameters of the two phases break different symmetries. But the theory of DQCP predicts a continuous phase transition between these two phases. At the DQCP, deconfined fractionalized spin excitations emerge and enhanced symmetry allows continuous rotation between the order parameters of the two ordered phases.

The DQCP in two-dimensional (2D) systems has been studied extensively and theoretically.[8–18] Although enormous computational cost are needed to clarify the unusual critical properties and deconfined fractionalized excitation emergent at the DQCP, numerical evidences are cumulated. Currently, most studies are based on several sophisticatedly designed models. To realize a DQCP in realistic 2D spin models or even in experimental quantum magnets[19] is, however, still a challenging task. Recently, some works studied possible DQCP in one-dimensional (1D) spin systems and obtained some interesting results.[20–32] An advantage of the 1D quantum spin systems over their 2D counterparts is that many powerful and well controlled analytical and numerical techniques, such as Bethe-ansatz, bosonization, and density matrix renormalization group (DMRG)[33–35] can be applied, and hence the results are more convincing. Meanwhile, enhanced quantum fluctuations in 1D employ strong constraint to ground-state properties, as involved in the Lieb–Schultz–Mattis (LSM) theorem.[36–38] It is recently noticed that this may help in stabilizing a DQCP in 1D.[26]

For an $S = 1/2$ chain with SO(3) spin rotational and lattice translational symmetries, the LSM theorem[36] implies that the ground state either breaks the translational symmetry to form a VBS or keeps plainly gapless. When generalized to systems with discrete symmetries, this theorem dictates that the ground state can not be symmetric and plainly gapped. Let us consider a system with two distinct discrete symmetries and assume a single tuning parameter can drive the system from one SSB phase to the other. At the transition point the symmetries restore and are often enhanced to allow continuous rotation between the two order parameters. According to the LSM theorem, the ground state at this point must be gapless, and in 1D, this implies the transition point is a DQCP. In many systems, the microscopic Hamiltonian contains such

†Corresponding author. E-mail: rong.yu@ruc.edu.cn

© 2022 Chinese Physical Society and IOP Publishing Ltd

a symmetry-enhanced point by properly tuning the model parameter. For example, the XY model consists of an isotropic point with continuous spin U(1) symmetry by tuning the spin anisotropy. Constrained by the LSM theorem, in 1D models, these symmetry-enhanced points exhibit properties that are eligible for a DQCP. This is a special case in 1D, as discussed later in this paper. In another class of systems, the enhanced symmetry can not be explicitly read off from the microscopic Hamiltonian, but emerges as both SSB order parameters are simultaneously suppressed by fluctuations. At the same time, the deconfined fractionalized excitations emerge, making this symmetry-enhanced point a DQCP. This case is more generally discussed in both 1D and 2D.

In this work, we investigate the dynamical signatures of the deconfined fractionalized excitations and enhanced continuous symmetry of two types of DQCP in 1D by studying an $S = 1/2$ spin chain with FM nearest-neighbor and AFM next nearest-neighbor interactions. We calculate the static and dynamic spin correlations by using the time evolution of infinite matrix product states (MPS). We show the existence of emergent continuous symmetries and characteristic of fractionalized excitations at two different DQCPs. At the DQCP between the VBS and FM phases, our calculation of dynamic structure factors suggests there is an effective spin–charge separation. While at the DQCP between the X-direction and Z-direction FM phases, we observe two different types of continua associated to different deconfined fractionalized excitations. Our results show direct evidence for the DQCP in 1D and provide valuable information in understanding the nature of the DQCP in both 1D and 2D.

2. Model and methods

To study the properties of DQCP in 1D, we consider an $S = 1/2$ spin chain with the following Hamiltonian:

$$H = \sum_i \left(-J_x S_i^x S_{i+1}^x - J_z S_i^z S_{i+1}^z\right) + K\left(S_i^x S_{i+2}^x + S_i^z S_{i+2}^z\right). \quad (1)$$

Here J_x and J_z are nearest-neighbor FM exchange interactions and K refers to the next nearest-neighbor AFM exchange coupling. This model has the $\mathbb{Z}_2^x \times \mathbb{Z}_2^z$ spin rotational symmetry, as well as the time reversal and lattice translational symmetries. It supports an X-direction FM, a Z-direction FM, and a VBS in the ground-state phase diagram as depicted in Fig. 1(a). In this work, we set $J_x = 1$ as the energy unit and study two quantum phase transitions: one along the blue arrow (by fixing $J_z = 1.5$ and increasing K) and the other along the red arrow (by fixing $K = 0$ and decreasing J_x), as shown in Fig. 1(a), respectively.

This model has been analyzed by using several different approaches.[20,25,26,30] Reference [30] has numerically confirmed that the ground states include a Luttinger liquid, a VBS phase, and a vector chiral phase sequently by increasing K along the isotropic line ($J_x = J_z$). Various field theory descriptions of the DQCPs between the FM and VBS phases have been discussed in detail in Ref. [26]. Another interesting analogy is mentioned in Refs. [26,30] that the VBS phase can be viewed as a symmetry-protected topological (SPT) phase by considering unit cells of two lattice sites. However, this SPT-like phase is obviously topologically trivial when examining the edge mode, given that the VBS is a SSB phase. But for the case of an infinite chain, the edge is unimportant, and therefore this analogy can make senses.

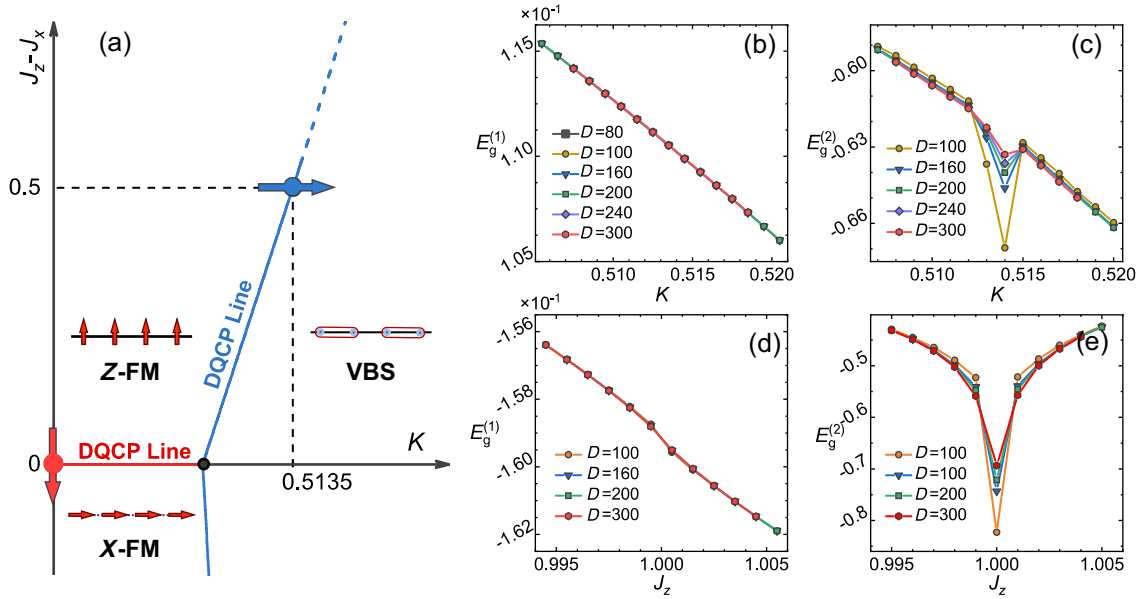


Fig. 1. (a) A schematic phase diagram of the model in Eq. (1). The isotropic line with quasi-long-range (QLR) order (red line) separates the X-direction and Z-direction ferromagnetic (FM) phases, i.e., a DQCP line. The DQCP line between the FM and VBS phases (blue solid line) with emergent O(2) × O(2) symmetry has been studied in Ref. [20]. A more complete phase diagram is mentioned in Ref. [25]. Here, we just focus on these two deconfined transitions (go through red line or blue line) without examining the properties over the entire phase diagram. (b) The first derivative $E_g^{(1)}$ of the ground-state energy with K along the blue arrow in panel (a). (c) The second derivative $E_g^{(2)}$ of the ground-state energy with K along the blue arrow in panel (a). (d) and (e) Same to (b) and (c) but along the red arrow.

An anisotropic O(4) non-linear sigma model (NLSM) with the Wess–Zumino–Witten term has been proposed to describe the scaling behaviors and emergent symmetry of the DQCP between the FM and VBS phases.[20] Here, to gain further understanding on the symmetry and fractionalized excitations of the two DQCPs, we apply the celebrated Jordan–Wigner (JW) transformation to this spin model and map it into interacting spinless fermions. The Hamiltonian in the fermion representation then reads

$$H = H_0 + H_{\rm int}, \tag{2}$$

where

$$H_0 = -\frac{J_z+J_x}{4}\sum_i \hat{T}_i - \frac{J_z-J_x}{4}\sum_i \left(f_i^\dagger f_{i+1}^\dagger + f_{i+1}f_i\right), \tag{3}$$

$$H_{\rm int} = -\frac{K}{2}\sum_i \left(\hat{T}_i - \hat{T}_{i+1}\right)^2 + K\sum_i \left(\hat{N}_i - \hat{N}_{i+1}\right)^2. \tag{4}$$

Here f_i is the annihilation operator for fermions on site i, $\hat{T}_i$ and $\hat{N}_i$ refer to the nearest-neighbor hopping and on-site particle number operators, respectively, defined as

$$\hat{T}_i = f_i^\dagger f_{i+1} + f_{i+1}^\dagger f_i = 2\left(S_i^x S_{i+1}^x + S_i^z S_{i+1}^z\right), \tag{5}$$

$$\hat{N}_i = f_i^\dagger f_i = \left(\frac{1}{2} + S_i^y\right). \tag{6}$$

The H_0 corresponds to the nearest-neighbor term of Eq. (1). The interaction term $H_{\rm int}$ is transformed from the next nearest-neighbor term of the spin model. Note that $\hat{T}_i$ is defined "on-bond" and $\hat{N}_i$ is defined "on-site".

In this work, we adopt the infinite time-evolving block decimation (iTEBD)[39,40] method to study the ground-state properties and zero-temperature space–time correlations of the spin model defined in Eq. (1). We focus on the critical behaviors near the two transitions as shown in Fig. 1(a). The matrix product representation is known to be accurate and efficient for gapped systems when the truncation dimension (Schmidt rank) D is large enough. In the situation where the system is gapless, the matrix product representation can still be applied and it provides a finite-gap (or finite-entanglement) variational state of a gapless system. With various well developed finite correlation length or finite-D scaling techniques, MPS representation is capable of exploring the critical properties trustingly.[41–43]

In the iTEBD method, one usually starts from a random initialization. Deep inside an ordered phase, the ground state is not sensitive to the way of initialization. The local order parameters and ground-state energy can be determined sufficiently accurate at a finite D. However, when the system is close to a critical point, finite-D effects may appear. There are usually two issues. The first issue is related to the emergent symmetry at the transition. Near the transition point, the emergent symmetry will give rise to many nearly degenerate ground state configurations, which are local minima in the variational approach. To avoid being trapped in a local minimum, our optimization procedure starts with many different initializations and the state with the lowest energy in the optimization is selected as the ground state. As a second issue, the gap obtained in a finite-D MPS is always finite. To solve this problem, we apply the well developed finite entanglement scaling technique, which allows to accurately locate the critical point from extrapolation.

For a state with a finite D, a finite gap presents because of the finite correlation length $\xi(D)$. To eliminate the effects of the finite-D gap to the critical exponents, we adopt a self-consistent method to determine the critical exponents. Applying the finite correlation length scaling approach, the critical exponents and the scaling function can be obtained from data collapse for different D's. We then use the fitted results to do a power-law fitting for the data with the largest correlation length, from which the critical exponents are reestimated. This procedure then repeats until the evaluated exponents are converged. Details of this self-consistent scaling method is elaborated in Appendix B.

The dynamical structure factors are calculated from the Fourier transforms of the space–time correlations. The calculation of space–time correlations is based on the real-time evolution of the ground-state MPS.[44] The computational cost of calculating the space–time correlations is much higher than optimizing a ground state. To keep the balance between truncation error and energy resolution, in this work, we adopt a fourth-order Trotter expansion of the real-time evolution operator, which leads to the energy resolution less than $10^{-3}J$.

3. Ground-state phase diagram and symmetries at the DQCPs

The schematic phase diagram of the model defined in Eq. (1) is presented in Fig. 1(a). For $J_z > J_x$ and small K the ground state is a FM with spin ordered along the S^z direction (denoted as the Z-direction FM). Since the model is symmetric under the $x \leftrightarrow z$ interchange, the ground state is an X-direction FM for $J_z < J_x$ and small K. For sufficiently large K, the ground state is a VBS that breaks the translational symmetry. The X-direction and Z-direction FM states meet at the isotropic line $J_z = J_x$ where the spin rotational symmetry of the Hamiltonian is enhanced from $\mathbb{Z}_2^x \times \mathbb{Z}_2^z$ to U(1). Constrained by the LSM theorem, along this line, the ground state preserves the U(1) symmetry and keeps to be gapless. Across this line from the X-direction FM to the Z-direction FM by tuning the parameter $J_z - J_x$ in the model, the system undergoes a continuous transition. At the transition point, the low-energy excitations are described by JW fermions. The JW fermions are deconfined with the enhanced U(1) symmetry, and can be viewed as the fractionalized excitations of domain walls (DWs), just like the marons or instantons for vortex in 2D. Therefore, the phase boundary between the X- and Z-direction

FM phases (red line in Fig. 1(a)) can be regarded as a line of DQCPs.

The transition between the Z-direction FM and VBS phases is driven by the next nearest-neighbor coupling K. It has been proposed that DQCPs with emergent $\mathrm{O}(2)\times\mathrm{O}(2)$ symmetry exist along the FM and VBS phase boundary (the blue line in Fig. 1(a)).[20,25,26] To understand the origin of the enhanced continuous symmetry, we examine the system in the JW fermion representation. The transition is controlled by H_{int} in Eq. (4), which contains an "on-bond" term (including $\hat{T}_i$) and an "on-site" term (including $\hat{N}_i$). Relevance of the "on-bond" term will cause breaking the translational symmetry on bonds and preserving all on-site symmetries, and therefore form a VBS. By contrast, the relevance of the on-site term will cause breaking the translational symmetry on sites and preserving all on-bond symmetries. This would result in a Y-direction AFM phase. For sufficiently large K in this model, the ground state prefers to a VBS instead of a Y-AFM state. In the continuous limit, these two terms of H_{int} correspond to the same order of interaction but pinning down different ordered states. There are also two sets of rotational symmetries originated from the on-bond and on-site symmetries, respectively. Interestingly, with proper tuning, the on-bond and on-site terms can be simultaneously marginal, which cause the enhanced $\mathrm{O}(2)\times\mathrm{O}(2)$ symmetry. Note that these emergent continuous symmetries at the transition is not possessed by the microscopic Hamiltonian of Eq. (1). This is a key difference from the transition across the boundary of the two FM phases. However, due to the LSM theorem in 1D, they share many similar features, and are both eligible for DQCPs.

4. Critical properties at DQCPs

We first examine the critical properties of the Z-direction FM to VBS transition. The ground-state energy E_{g}, its first derivative $E_{\mathrm{g}}^{(1)} = \mathrm{d}E_{\mathrm{g}}/\mathrm{d}K$, and the second derivative $E_{\mathrm{g}}^{(2)} = \mathrm{d}E_{\mathrm{g}}^{(1)}/\mathrm{d}K$ have been calculated. As demonstrated in Figs. 1(b) and 1(c), $E_{\mathrm{g}}^{(1)}$ varies continuously across the transition, and $E_{\mathrm{g}}^{(2)}$ develops a singularity at the transition point ($K \approx 0.5135$), featuring a continuous transition. We further calculate the order parameters $m_z = \sum_i \langle S_i^z \rangle / N$ and $\Psi = \sum_i \langle | \Psi_i - \Psi_{i+1} | \rangle / N$ of the Z-FM and VBS phases, respectively, to verify the continuous nature of the transition. A more concrete definition of the order parameters is listed in Table 1. As shown in Fig. 2(a), m_z and Ψ both exhibit near-continuous transitions at the same point, consistent with the results of ground-state energy, giving robust evidence of a DQCP. It is worth noting that at any finite-D, both order parameters take small finite values at the transition point. This finite-D effect is inherent in the MPS approximation of the long-range entangled gapless state, as mentioned in the previous section. To obtain the behavior of order parameters in the thermodynamic limit, we extrapolate their values in the large-D limit, as also shown in Fig. 2(a). Indeed, both order parameters are continuously suppressed to zero at the same K value.

Figures 1(d) and 1(e) show the derivatives of ground-state energy across the X-FM to Z-FM transition. The results are similar to those in Figs. 1(b) and 1(c). Meanwhile, the order parameters of the two SSB phases, m_z and m_x, both drop down to zero at the transition point simultaneously, as shown in Fig. 2(b). These results evidence a continuous transition, and imply that the symmetry is enhanced to U(1) at the transition point, which is consistent with the LSM theorem. Besides the similar behaviors in the order parameters, we find the central charges of the two transitions are both close to 1 (see Fig. 2(c)), which belong to the free boson universality class.[45,46] This does not mean the low-energy excitations are bosonic, but implies that they arise from fractionalizing the bosonic modes, which is a feature of DQCP.

To further show the two transitions are eligible for DQCPs, we further calculate the correlation functions to verify the existence of emergent continuous symmetry and global topological conservation. The gauge constraint at the DQCPs guarantees the conservation of the Noether current, $\partial_\mu \mathcal{J}^\mu = 0$, which implies that the anomalous exponents of the conserved currents must be pinned to $\eta = 2$, and the current–current correlation in energy–momentum space must be gapless and linear.

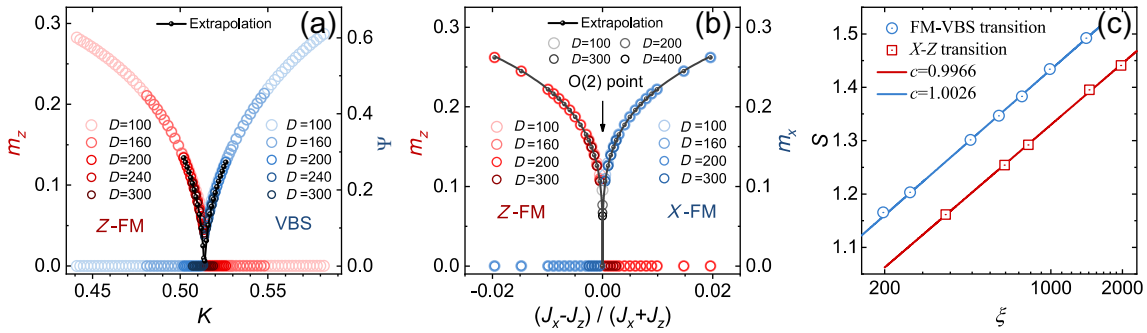


Fig. 2. (a) The Z-FM order parameter m_z and VBS order parameter Ψ versus K at $J_z - J_x = 0.5$. (b) Z-FM order parameter m_z and X-FM order parameter m_x versus $(J_x - J_z)/(J_x + J_z)$ at $K = 0$. (c) Scaling of the entanglement entropy S with effective correlation length ξ. The central charge is extracted from the slope of a linear fit.

Table 1. Identification of the vector components and conserved currents for different emergent O(2) symmetries.

Transition	Channel	Vector components	Conserved current
FM–VBS	$O(2)_c$	$S_i^{z,u} = S_i^z + S_{i+1}^z$ $\Psi_i = S_i^x S_{i+1}^x + S_i^z S_{i+1}^z - S_i^y S_{i+1}^y$	$\mathcal{J}_i^c = S_i^x S_{i+1}^y + S_i^y S_{i+1}^x$
	$O(2)_s$	$S_i^{x,u} = S_i^x + S_{i+1}^x$ $S_i^{y,s} = S_i^y - S_{i+1}^y$	$\mathcal{J}_i^s = S_i^z - S_{i+1}^z$
X–Z	$SU(2)_c$	$S_i^{y,u} = S_i^y + S_{i+1}^y$ $\Gamma_i = S_i^z S_{i+1}^x + S_i^x S_{i+1}^z$ $\Phi_i = S_i^x S_{i+1}^x - S_i^z S_{i+1}^z$	Φ_i, Γ_i, and $S_i^{y,u}$
	$O(2)_s$	S_i^z S_i^x	$\mathcal{J}_i^s = S_i^y$

The vector components and conserved currents of emergent symmetries are listed in Table 1. For the FM–VBS DQCP, it has been proposed that there are two emergent O(2) symmetries.[20] In the spinon language, the continuous rotation of uniform S^x and staggered S^y is the gauge symmetry on site with spin flip and the rotation of S^z and Ψ is the gauge symmetry on bond without spin flip. Thus, we can regard the rotation of uniform S^x and staggered S^y as an effective "spin" sector, labeled as $O(2)_s$. On the other hand, the rotation of S^z and Ψ form an effective "charge" sector, labeled as $O(2)_c$. As shown in Figs. 3(a) and 3(b), although these two different O(2) symmetries keep different anomalous exponents, their conserved currents both follow a scaling law of $\mathcal{J} \sim r^{-2}$ and in each sector (charge or spin) the two vector components behave with the same scaling dimension. Besides, an additional result $\eta_c \eta_s \approx 1$ validates the prediction of field theory in Ref. [20].

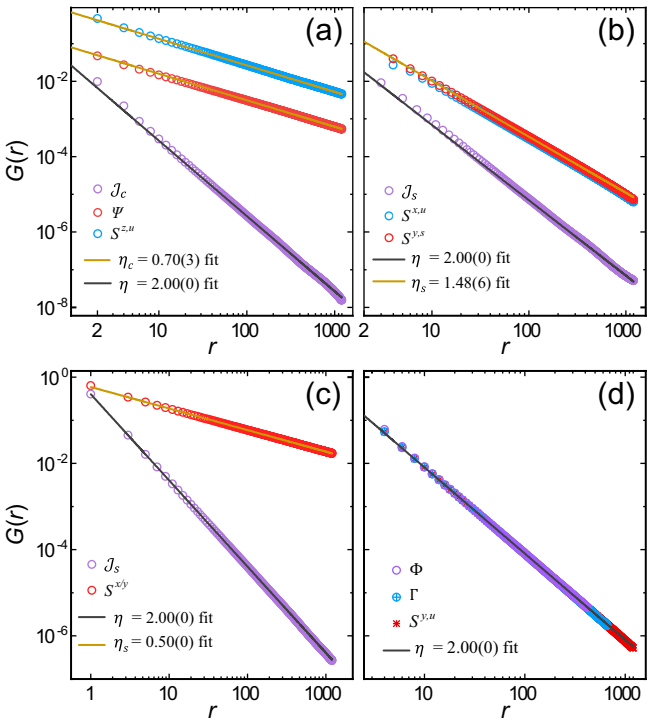


Fig. 3. Correlation functions of the emergent conserved currents and vector components for (a) $O(2)_c$ of the FM–VBS transition, (b) $O(2)_s$ of the FM–VBS transition, (c) $O(2)_s$ of the X–Z FM transition, and (d) $SU(2)_c$ of the X–Z FM transition.

For the transition between the two FM states at the isotropic point with $J_x = J_z$, there is an enhanced $U(1) \sim O(2)$ symmetry. As demonstrated in Fig. 3(c), the scaling law of $S_y \sim r^{-2}$ reflects the global conservation of the JW fermion number. It can also be regarded as the conserved current of the X–Z rotation, labeled as $O(2)_s$. To further illustrate the notion of deconfinement, we show that another $SU(2)_c$ symmetry listed in Table 1 is also emergent at the DQCP of the X–Z transition. As demonstrated in Fig. 3(d), the anomalous exponents of these three operators are all pinned at an integer of 2, which indicates an emergent SU(2) symmetry.

5. Dynamical signatures of DQCPs

Results in previous sections only provide evidences for continuous FM–FM and FM–VBS transitions, based on which the DQCPs are implied. To directly show the existence of deconfined fractionalized excitations at the DQCPs, we calculate the space–time correlations of conserved currents and spin components by real-time evolution of the ground-state MPS. After Fourier transforms of the space–time correlations, we can get a dynamical spectrum in the energy–momentum space.

As demonstrated in Figs. 4(a) and 4(b), the current–current correlations in energy–momentum space at the transition points are indeed gapless with linear low-energy dispersion. At the FM–VBS transition, the two emergent symmetries $O(2)_c$ and $O(2)_s$ can be identified from the "charge" and "spin" channels separately, and they have the same Fermi velocity. Combining these results with the analysis of anomalous exponents above, we can safely confirm that there exist two emergent symmetries. At the DQCP of the X–Z FM transition, S^y is the conserved current of the S^x–S^z rotation as well as of the Φ–Γ rotation. The existence of two continuous symmetries at the X–Z FM transition is also confirmed.

The signatures of deconfined fractionalized excitations at the FM–VBS DQCP are illustrated in Fig. 5 clearly. Approaching to the DQCP from either side, we observe the development of two sets of continuous spectra (panels in the upper and lower rows of Fig. 5). As shown in Figs. 5(b) and 5(e), they both become gapless at the DQCP. Near the zone center, these two continua are bounded by the same edge (linear in the momentum k). However, when going away from the zone

center by increasing k, they are separated with two independent edges. Note that these two modes are associated with effective "charge" and "spin" channels, respectively. Therefore, this is the signature of an effective spin–charge separation of the system. The spin–charge separation is common in 1D Luttinger liquid. In the long wave length limit, the interaction terms causing charge (VBS) and magnetic (Z-FM) orders are all irrelevant under renormalization group (RG) flow, which signifies free fermion excitations. However, as the momentum k increases, the effect of the scattering processes lead to the separation of spin and charge excitations. In the case of the easy-plane DQCP in 2D proposed by Senthil *et al.*, the spinons (fractions of S^+) and merons (fractions of skyrmions) are deconfined simultaneously, in a way analogous to the spin and charge excitations discussed here.

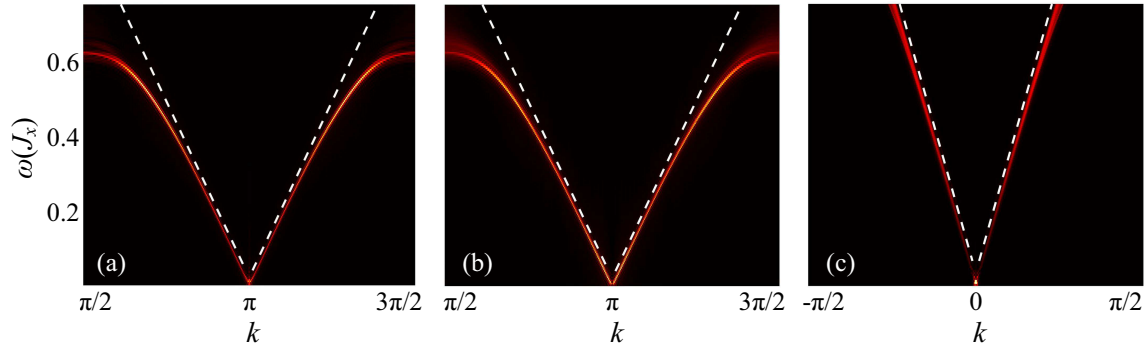


Fig. 4. Low-energy spectra of the dynamic current–current correlations listed in Table 1. (a)–(c) Correlations of $\mathcal{J}^c$ at the FM–VBS transition, $\mathcal{J}^s$ at the FM–VBS transition and S^y at the X–Z FM transition, respectively. The white lines are fits to the linear dispersion.

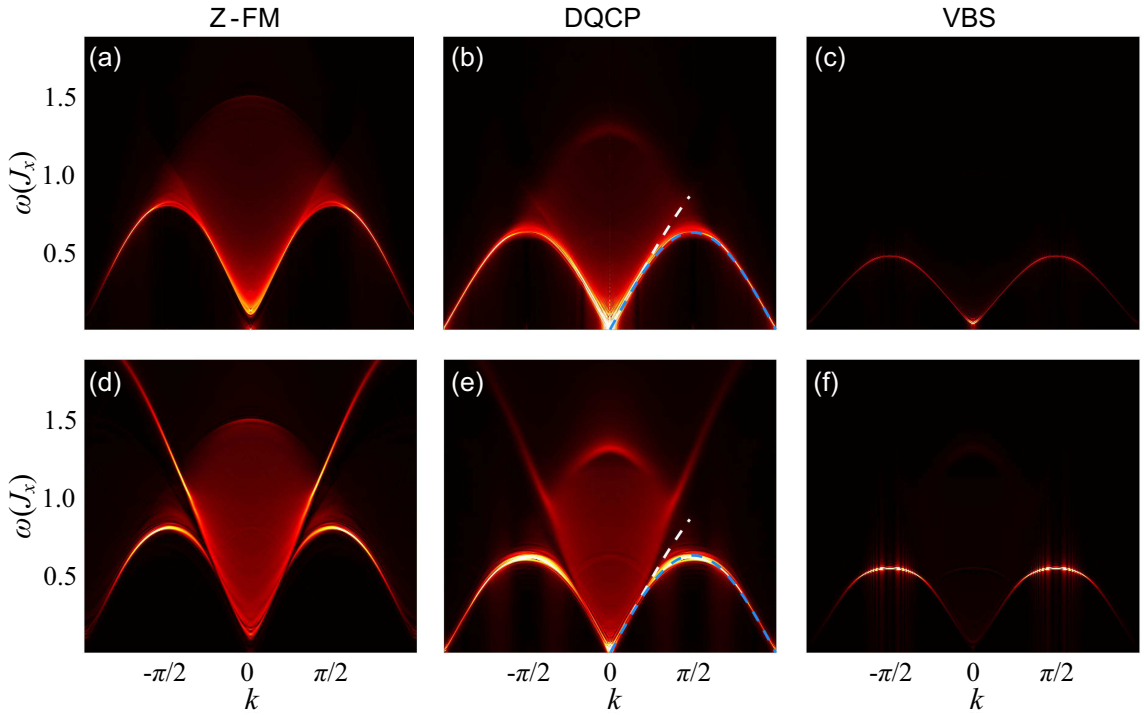


Fig. 5. Dynamic spin structure factors of (a)–(c) the S^z channel and (d)–(f) the S^x chanel. Panels (a) and (d) are inside the Z-FM phase. Panels (b) and (e) are at the DQCP. Panels (c) and (f) are inside the VBS phase. The blue and white dashed lines in (b) and (e) trace out the two bright bound edges from (b) and are guides to eyes in (e).

The excitations at the X–Z FM DQCP are clearer. The continuum showed in Fig. 6(a) is conspicuous with clear boundaries. In the JW fermion representation, it is nothing but the particle–hole excitations of the free fermions. The topological excitations (JW particles) are totally deconfined at any length scale. The clear boundary is the sign of a well defined Fermi surface. The continuum of the S^xS^z channel in Fig. 6(c) can also be regarded as a measure of the topological excitations and it is a folding of the continuum in Fig. 6(a). In the S^x (or S^z) channel, the gapless point of the continuum appears at $k = 0$ and the boundary of the continuum is indistinct as demonstrated in Fig. 6(b), which is different from the behavior in the S^y channel. The excitation spectrum shown in the $S^{x/z}$ channel suggests a Dirac cone like Fermi surface. At a first glance this is surprising because the model at this point is mapped to non-interacting JW fermions. However, we note

that the JW transformation itself is nonlocal, and the $S^{x/z}$ channel just happens to probe the inherent many-body effects. This is a unique feature of 1D systems.

The anomalous exponents of S^x, S^y, and S^xS^z have been calculated in the previous section. Different η values are also characterized in the dynamical structure factors. For $\eta = 0$, the excitation spectrum would contain a bright bound state. For $\eta = 1$, which corresponds to the free JW fermions,[35] the spectrum should exhibit a smooth continuum just like the one shown in Fig. 6(a). And for $\eta = 2$, at a fixed momentum k, the spectral weight will vanish at $\omega = 0$ and increase linearly with the frequency ω, just like the continuum near $k = \pm\pi$ in Fig. 6(c). For the correlations of S^x, $\eta = 0.5$. The dynamical structure factor of this channel, as shown in Fig. 6(b), exhibits a continuum with a bright edge, consisting of characters of excitations at both $\eta = 0$ and $\eta = 1$.

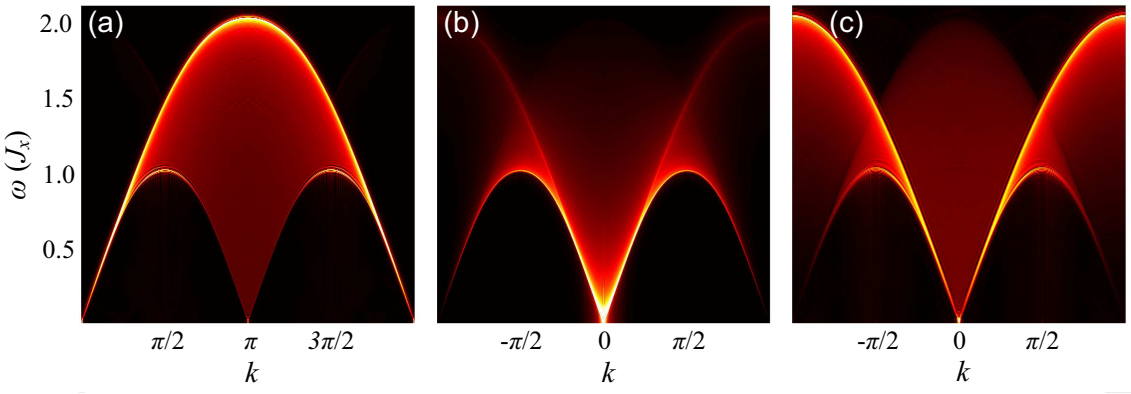


Fig. 6. Dynamic structure factors of (a) S^y channel, (b) S^x channel, and (c) S^xS^z channel at the DQCP of the X–Z FM transition.

6. Discussion and conclusions

As mentioned in the introduction, the realization of a DQCP in 2D spin systems without fine-tuning is still challenging and the enormous computational cost limits detailed analysis of the critical properties, especially the dynamical ones. As a reasonable instead, we numerically study the critical properties of 1D DQCPs in detail. We show that the model in Eq. (1) contains two types of DQCPs, which are located at the VBS–FM and the X–Z FM transitions, respectively. They share many similar critical properties that are eligible for DQCPs, despite the different underlying mechanisms and symmetry aspects. These key differences are clearly reflected in the calculated dynamic spectra of different spin channels, which are firstly explored in this work. The gapless and linear dispersions of the current–current correlations in energy–momentum space further verify the existence of emergent symmetries. At the VBS–FM DQCP, our calculation of dynamic spin structure factors give robust evidence of spin-charge separation. And at the X–Z FM DQCP, besides the JW fermion continuum, another type of fractionalized excitation is observed.

In the field theory description, these two different types of DQCPs can both be described by the same low-energy effective model — the sine-Gordon model,[47] although their microscopic Hamiltonians' symmetries are totally different. In this sense, the ground states exactly on these two lines both exhibit Luttinger liquid behavior at low energies. As expounded in Section 5, the low-energy excitations for these two DQCPs do not show notable difference, qualitatively. On the other hand, the spin–charge separation takes place at higher energy and larger momentum, for which the dispersions show distinct nonlinear behavior and hence beyond the field theory description. There are also other additional modes for the FM–VBS DQCPs at much higher energy. It would come as no surprise because this energy scale is far beyond the field theory capability and thus the different symmetries embodied in microscopic Hamiltonians will lead to different excitation modes. Nevertheless, the different excitation modes at higher energy may contain some interesting consequences beyond the low-energy view at present and it would inspire us to develop more analytical approaches for larger energy scale.

Our results also verify the important role of the LSM theorem played in stabilizing the 1D DQCP. At the transition point between the X-FM and Z-FM phases, the symmetry of the Hamiltonian is enhanced to U(1). Constrained by the LSM theorem, the ground state at this point should preserve the symmetry and be gapless. Although LSM theorem does not rule out a first-order transition between the two SSB phases in general, the unique feature of 1D system excludes the possibility of a Goldstone mode. Therefore, a first-order transition with an enhanced continuous symmetry can not take place in 1D, and the system must undergoes a continuous transition, namely, via a DQCP. As discussed, this type of DQCP can only be realized in 1D systems. In higher dimensions, emergent Goldstone mode associated with the enhanced symmetry appears and the transition is usually of first order. On the other hand, the enhanced continuous symmetry at the DQCP between the FM and VBS phases emerges only in the long wave length. This type of DQCP is not limited in 1D.

In summary, using the iTEBD method, we study the critical properties as well as the dynamical spectra of two types of

1D DQCP in an $S = 1/2$ spin chain. The scaling of the correlation functions and the dispersion of the conserved current correlations explicitly show the emergence of enhanced continuous symmetries at the two different DQCPs. The dynamical signatures of the spin excitation spectra reveal deconfined fractionalized excitations at the DQCPs. We also find an effective spin–charge separation at the DQCP between the the FM and VBS phases, and identify two continua associated with different types of fractionalized excitations at the DQCP between the X-direction and Z-direction FM phases. Our results uncover rich physics of the DQCP in 1D and help understand the nature of DQCP in higher dimensions.

Appendix A: Some useful Lie algebras

Here we summarize some local Lie algebras in Table A1. They are useful in defining the order parameters and when approaching to a DQCP, global topological conservation laws arise. The on-site spin SU(2) algebra is obvious and denoted as $\mathrm{SU(2)_s}$ in Table A1. Besides, there are also two sets of on-bond algebras. There are four basis states in a two-site unit cell, $(|\uparrow\uparrow\rangle, |\downarrow\downarrow\rangle, |\uparrow\downarrow\rangle, |\downarrow\uparrow\rangle)$, and we can separate them into two parts, $(|\uparrow\uparrow\rangle, |\downarrow\downarrow\rangle)$ and $(|\uparrow\downarrow\rangle, |\downarrow\uparrow\rangle)$, for which the numbers of domain walls (dw) contained are 0 and 1, respectively. The operators $v^{\alpha}_{i,j}$ $(\alpha = 1,2,3)$ defined in Table A1 form a closed SU(2) Lie algebra in the dw $= 0$ space $(|\uparrow\uparrow\rangle, |\downarrow\downarrow\rangle)$, and is therefore denoted as $\mathrm{SU(2)_{dw0}}$. While the operators $\tau^{\alpha}_{i,j}$ also form a closed SU(2) algebra in the dw $= 1$ space, which is denoted as $\mathrm{SU(2)_{dw1}}$. All these operators listed in Table A1 can not mix the spaces between dw $= 0$ and dw $= 1$, namely, they preserve the number of domain walls locally.

Table A1. Related SU(2) Lie algebras in this work.

Symmetries	Generators		
$\mathrm{SU(2)_{dw1}}$	$\tau^1_{i,j} = \frac{1}{2}(\sigma^x_i\sigma^x_j + \sigma^y_i\sigma^y_j)$	$\tau^2_{i,j} = \frac{1}{2}(\sigma^y_i\sigma^x_j - \sigma^x_i\sigma^y_j)$	$\tau^3_{i,j} = \sigma^z_i - \sigma^z_j$
$\mathrm{SU(2)_{dw0}}$	$v^1_{i,j} = \frac{1}{2}(\sigma^x_i\sigma^x_j - \sigma^y_i\sigma^y_j)$	$v^2_{i,j} = \frac{1}{2}(\sigma^y_i\sigma^x_j + \sigma^x_i\sigma^y_j)$	$v^3_{i,j} = \sigma^z_i + \sigma^z_j$
$\mathrm{SU(2)_s}$	σ^x_i	σ^y_i	σ^z_i

Appendix B: Finite entanglement scaling

For a matrix product state with a finite D, the finite gap is associated to a finite effective correlation length $\xi(D)$. This effective correlation length can be calculated from the correlation structures of the MPS. The static correlation of two operators u and v in the MPS language reads[40]

$$\begin{aligned}\langle u(0)v(r)\rangle &= LT_uT^{r-1}T_vR\\ &= L_uT^{r-1}R_v,\end{aligned} \tag{B1}$$

where T is the transfer operator, L and R are the left and right eigenvectors of T with the largest eigenvalue, respectively. This process can be expressed in a more intelligible tensorgraph representation as demonstrated in Fig. B1.

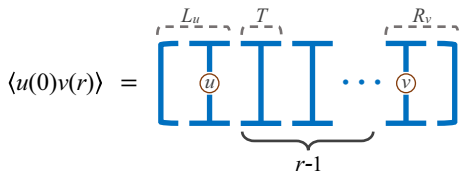


Fig. B1. Graph representation of two-point correlators.

Typically, the transfer operator T is a symmetric matrix (corresponding to the space-inversion symmetry) and it can be diagonalized with real eigenvalues. Two-point correlators $\langle u(0)v(r)\rangle$ can be transformed as follows:

$$\begin{aligned}\langle u(0)v(r)\rangle &= L_uU^{-1}\Lambda^{r-1}UR_v\\ &= \Lambda_1^{r-1}\left[c_1 + \sum_{k=2}^{\mathrm{rank}(T)} c_k(\Lambda_k/\Lambda_1)^{r-1}\right],\end{aligned} \tag{B2}$$

where Λ_k are the eigenvalues of the transfer operator T and Λ_1 is the largest eigenvalue. If we transform the transfer operator into a normalized form with $\Lambda_1 = 1$, there remains a constant term c_1 and an exponential decay term $\sum c_k\Lambda_k^{r-1}$ in Eq. (B2). The constant term guarantees the long range order. The leading decay factor $\gamma = \Lambda_2$ (the second largest eigenvalue) contributes to an effective correlation length $\xi = -1/\ln(|\gamma|)$.

If the truncation dimension D is sufficiently large, the effective correlation length λ can be taken as the real correlation length for a gapped state. Nevertheless, for a gapless state, this exponential decay factor always presents, which leads to a finite-D deviation from the true value at the thermodynamic limit.

The finite correlation length scaling of correlation function near the critical point reads

$$G(r,\xi) = \frac{\exp(r/\xi)}{r^{\eta}}f(r/\xi), \tag{B3}$$

where η is the anomalous exponent and $f(r/\xi)$ is a homogeneous scaling function. For the matrix product representation, the exponential decay factor exists all along even in a gapless state. Even so, close to the transition point, the power-law term will dominate the scaling behavior of the correlation function for $r < \xi$.

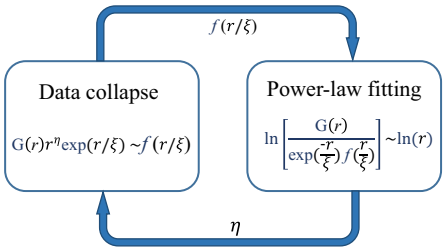


Fig. B2. Self-consistent process to extract the anomalous exponents.

Data collapse has been widely adopted to extract the anomalous exponents. However, it is often hard to judge the quality of data collapse. So it usually only provides some rough estimate of the exponents. Alternatively, one can also extract the anomalous exponents from a direct power-law fit to

the correlation functions. However, there are some practical issues for a direct fit because the sub-leading contribution in the scaling function $f(r/\xi)$ would have an effect on the accuracy of fitting for the short-range correlations and the exponential decay factor would ruin the power-law behavior of the long-range correlations. Here we adopt a way to extract the exponents by combining these two methods, and show that this will give refined estimates of the anomalous exponents. Specifically, direct power-law fitting can provide an initial value of the anomalous exponent η, and $f(r/\xi)$ fitted from data collapse can be used to promote the power-law fitting of the correlation function. This process is then repeated until a self consistence of η is obtained. The sketch of our method is illustrated in Fig. B2. The final fitting results of the anomalous exponents are illustrated in Fig. 3 of the main text. Examples of data collapse for G_x at the X–Z FM transition and G_Ψ at the FM–VBS transition are shown in Fig. B3, respectively.

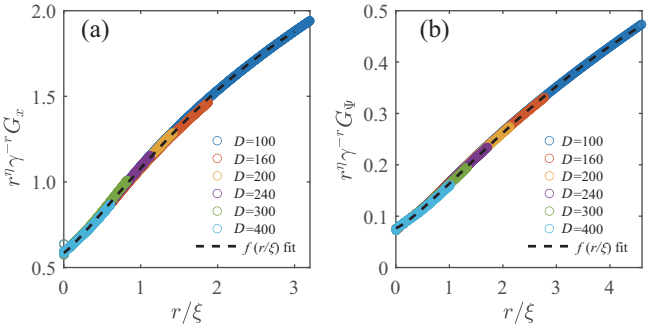


Fig. B3. Data collapse of the correlations functions for (a) S^x at the X–Z FM transition and (b) Ψ at the FM–VBS transition.

Appendix C: Calculation of dynamic structure factors

In this section, we briefly describe the process of calculating the dynamical structure factors in the matrix product representation. We first calculate the zero-temperature space–time correlation $\langle\hat{O}(0,0)\hat{O}(r,t)\rangle$ by using the iTEBD method. The calculation of the space–time correlation of unitary operators is a standard operation of iTEBD. The space–time correlation can be written as

$$\begin{aligned}\langle\hat{O}(0,0)\hat{O}(r,t)\rangle &= \langle\psi_G|\hat{O}(0)\,\mathrm{e}^{-\mathrm{i}t\hat{H}}\hat{O}(r)\,\mathrm{e}^{\mathrm{i}t\hat{H}}|\psi_G\rangle \\ &= \langle\psi_L|\,\mathrm{e}^{-\mathrm{i}t\hat{H}}\hat{O}(r)\,\mathrm{e}^{\mathrm{i}t\hat{H}}|\psi_G\rangle\,. \end{aligned} \tag{C1}$$

If the ground state $\langle\psi_G|$ is in the canonical form, the state $\langle\psi_L| = \langle\psi_G|\hat{O}(0)$ will also be in the canonical form, for $\hat{O}$ is a unitary operator. Then standard operations of the real-time evolution can be applied as shown in Fig. C1. After that, dynamical structure factor of $\hat{O}$ can be obtained by Fourier transformation of $\langle\hat{O}(0,0)\hat{O}(r,t)\rangle$.

In the practical calculation, a fourth-order Suzuki–Trotter decomposition method is applied to eliminate the time-step errors as possible. The values of the time step τ and number of steps N are experience-based decisions. A larger τ will result in a larger Trotter error and a smaller range of energy. There are also some practical problems to improve the energy resolution by taking a large number of steps. The truncation errors will increase with larger N, and the memory cost will grow quadratically with N. To keep balance between the computing resource and acceptable errors, in the calculation of the space–time correlations, we take the truncation dimension $D = 48$, the time step $\tau = 0.6J_x^{-1}$ (more accurate than $\tau = 0.04J_x^{-1}$ by second-order decomposition), and the number of steps $N = 1200$.

To trace out the low-energy linear dispersion in the k–ω space, we find out the ω values corresponding to the maximum of DSF for each k and then fit the k–ω data nearby the zoom center linearly. The linear guide lines in the main text are our linear-fitting results in this way and the boundary guide lines are direct plots of k–ω data.

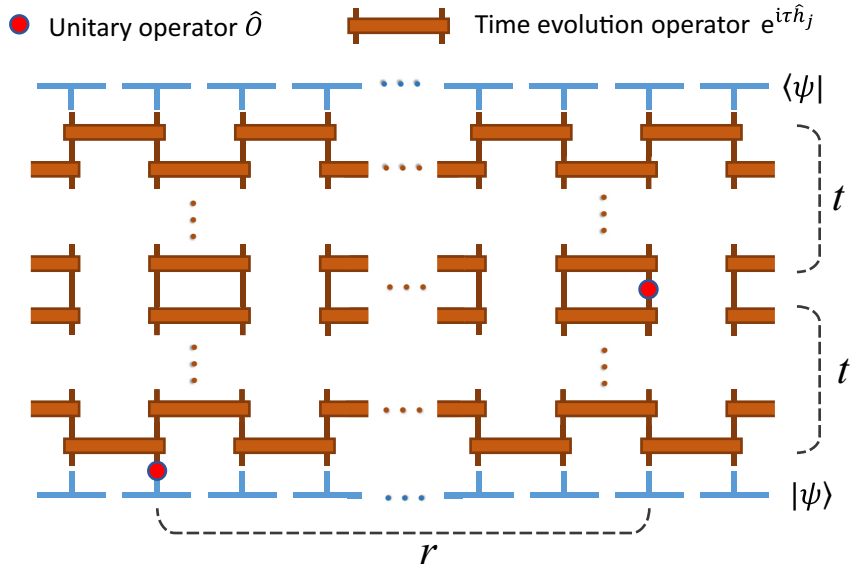


Fig. C1. Sketch of calculating the space–time correlation $\langle\hat{O}(0,0)\hat{O}(r,t)\rangle$ in the matrix product representation.

Acknowledgments

We thank Z. Y. Xie, Z. X. Liu, W. Q. Yu, Y. Wang, J. Wu, and C. L. Liu for useful discussions.

Project supported by the National Science Foundation of China (Grant No. 12174441), the Fundamental Research Funds for the Central Universities, China, and the Research Funds of Remnin University of China (Grant No. 18XNLG24).

References

[1] Chaikin P M and Lubensky T C 1995 *Principles of condensed matter physics* (Cambridge: Cambridge University Press)
[2] Giamarchi T 2004 *Quantum Physics in One Dimension* (Oxford: Oxford Univ. Press)
[3] Diep H T 2004 *Frustrated spin systems* (Beijing: World Scientific)
[4] Lacroix C, Mendels P and Mila F 2013 *Introduction to Frustrated Magnetism Materials, Experiments, Theory* (Berlin: Springer Berlin)
[5] Sachdev S 2011 *Quantum Phase Transition* (Cambridge: Cambridge University Press)
[6] Senthil T, Vishwanath A, Balents L, Sachdev S and Fisher M P A 2004 *Science* **303** 1490
[7] Senthil T, Balents L, Sachdev S, Vishwanath A and Fisher M P A 2004 *Phys. Rev. B* **70** 144407
[8] Sandvik A W 2007 *Phys. Rev. Lett.* **98** 227202
[9] Chen K, Huang Y, Deng Y, Kuklov A B, Prokof'ev N V and Svistunov B V 2013 *Phys. Rev. Lett.* **110** 185701
[10] Nahum A, Serna P, Chalker J T, Ortuno M and Somoza A M 2015 *Phys. Rev. Lett.* **115** 267203
[11] Shao H, Guo W and Sandvik A W 2016 *Science* **352** 213
[12] Qin Y Q, He Y Y, You Y Z, Lu Z Y, Sen A, Sandvik A W, Xu C and Meng Z Y 2017 *Phys. Rev. X* **7** 031052
[13] Ma N, Sun G Y, You Y Z, Xu C, Vishwanath A, Sandvik A W and Meng Z Y 2018 *Phys. Rev. B* **98** 174421
[14] Ma N, You Y Z and Meng Z Y 2019 *Phys. Rev. Lett.* **122** 175701
[15] Lee J Y, You Y Z, Sachdev S and Vishwanath A. 2019 *Phys. Rev. X* **9** 041037
[16] Xi N, Chen H, Xie Z Y and Yu R 2021 arXiv: 2111.07368
[17] Zhao B, Takahashi J and Sandvik A W 2020 *Chin. Phys. B* **29** 57506
[18] Sun G, Ma N, Zhao B, Sandvik A W and Meng Z Y 2021 *Chin. Phys. B* **30** 067505
[19] Cui Y, Liu L, Lin H, Wu K-H, Hong W, Liu X, Li C, Hu Z, Xi N, Li S, Yu R, Sandvik A W and Yu W 2022 arXiv:2204.08133
[20] Huang R Z, Lu D C, You Y Z, Meng Z Y and Xiang T 2019 *Phys. Rev. B* **100** 125137
[21] Huang R Z and Yin S 2020 *Phys. Rev. Research* **2** 023175
[22] Affleck I and Haldane F D M 1987 *Phys. Rev. B* **36** 5291
[23] Patil P, Katz E and Sandvik A W 2018 *Phys. Rev. B* **98** 014414
[24] Mudry C, Furusaki A, Morimoto T and Hikihara T 2019 *Phys. Rev. B* **99** 205153
[25] Roberts B, Jiang S and Motrunich O I 2019 *Phys. Rev. B* **99** 165143
[26] Jiang S and Motrunich O I 2019 *Phys. Rev. B* **99** 075103
[27] Yang S, Yao D X and Sandvik A W 2020 arXiv: 2001.02821
[28] Roberts B, Jiang S and Motrunich O I 2021 *Phys. Rev. B* **103** 155143
[29] Yang S and Xu J B 2021 *Phys. Rev. E* **104** 064121
[30] Furukawa S, Sato M, Onoda S and Furusaki A 2012 *Phys. Rev. B* **86** 094417
[31] Luo Q, Zhao J and Wang X 2019 *Phys. Rev. B* **100** 121111
[32] Sun G, Wei B B and Kou S P 2019 *Phys. Rev. B* **100** 064427
[33] White S R 1992 *Phys. Rev. Lett.* **69** 2863
[34] Delft J V and Schoeller H 1998 *Annalen der Physik* **7** 225
[35] Fradkin E 2013 *Field theories of condensed matter systems* (Cambridge: Cambridge University Press)
[36] Lieb E, Schultz T and Mattis D 1961 *Ann. Phys.* **16** 407
[37] Nomura K, Morishige J and Isoyama T 2015 *J. Phys. A* **48** 375001
[38] Isoyama T and Nomura K 2017 *Prog. Theoret. Experiment. Phys.* **2017** 103I01
[39] Vidal G 2007 *Phys. Rev. Lett.* **98** 070201
[40] Schollwöck U 2011 *Ann. Phys.* **326** 96
[41] Tagliacozzo L, Oliveira T R, Iblisdir S and Latorre J I 2008 *Phys. Rev. B* **78** 024410
[42] Pollmann F, Mukerjee S, Turner A M and Moore J E 2009 *Phys. Rev. Lett.* **102** 255701
[43] Pirvu B, Vidal G, Verstraete F and Tagliacozzo L 2012 *Phys. Rev. B* **86** 075117
[44] White S R and Affleck I 2008 *Phys. Rev. B* **77** 134437
[45] Latorre J I and Riera A 2009 *J. Phys. A* **42** 504002
[46] For a system with open boundary conditions, the scaling of the entanglement entropy reads $s \sim \frac{c}{6}\log(\xi)$, where c is the central charge.
[47] Xi N and Yu R 2022 arXiv: 2202.12543